Structure and magnetic property changes of epitaxially grown $L1_0$-FePd isolated nanoparticles on annealing

Kazuhisa Sato[a] and Yoshihiko Hirotsu
The Institute of Scientific and Industrial Research, Osaka University, 8-1 Mihogaoka, Ibaraki 567-0047, Osaka, Japan

(Received 28 October 2002; accepted 28 February 2003)

Isolated 10-nm-sized FePd nanoparticles with the $L1_0$-type ordered structure have been fabricated by electron-beam evaporation and postannealing above 773 K, and the structural details have been investigated by transmission electron microscopy. FePd particles were epitaxially grown on a cleaved NaCl(001) substrate and were two-dimensionally dispersed on the substrate. In FePd particles formation, Pd nanoparticles were first deposited as ''seed'' particles epitaxially on NaCl followed by a successive deposition of Fe particles. All the Fe particles were captured by Pd particles forming Fe/Pd nanocomplex particles with a mutual fixed orientation. Coalescence and growth of the particles were not prominent during annealing, indicating that the alloying and atomic ordering reactions proceeded mostly within each nanoparticle. The negligible coalescence can be attributed to an ''anchoring effect'' of the seed Pd to the coalescence growth. Moreover, both of these reactions are thought to proceed almost simultaneously during annealing at temperatures between 723 and 823 K. Most of the annealed particles were single crystal particles with *c* axes oriented both normal and parallel to the film plane. Large coercivities above 3 kOe were obtained after annealing at 873 K, though they were smaller than those expected from the theoretical model. The small coercivity value can be attributed to the low magnetocrystalline anisotropy. The magnetocrystalline anisotropy constant of the present FePd nanoparticles estimated was less than half of that of the bulk materials. © *2003 American Institute of Physics.*
[DOI: 10.1063/1.1568531]

I. INTRODUCTION

Magnetic recording density has been increasing every year and it has reached nearly the maximum value for conventional continuous magnetic storage media.[1–4] As future ultra-high-density recording media, one of the ideal candidates is thought to be the assembly of isolated hard magnetic nanoparticles with sizes smaller than 10 nm in an insulating film in order to increase the storage density and to reduce noise. These particles have a smaller particle diameter than their magnetic domain size, that is, single domain particles, so the magnetization process is carried by rotation magnetization. According to the Stoner–Wohlfarth (SW) model,[5] coercivity is expressed by the following relation:

$$H_c \approx \frac{K_u}{I_s}, \tag{1}$$

where H_c represents the coercivity, K_u the uniaxial magnetoanisotropy constant, and I_s the saturation magnetization. This model is based on such assumptions that coherent rotation of magnetization of single domain particles, which are randomly distributed with uniaxial magnetoanisotropy and without interparticle magnetostatic interaction of thermal fluctuation of magnetization. However, these assumptions are so strict that they are only valid in the case of magnetic particles with very strong magnetoanisotropy or at very low temperature. Actually, in ferromagnetic nanoparticles, the volume reduction generally causes thermal fluctuation of magnetization of particles,[6,7] which finally results in the appearance of superparamagnetism.[8] A criterion for the appearance of superparamagnetism can be discussed using the following relation, $K_uV \sim k_BT$, where V is the volume of the magnetic particle, k_B the Boltzmann constant, and T the temperature. On the other hand, this expression means that particles with high magnetocrystalline anisotropy can overcome thermal fluctuation even in the case of smaller-sized particles, giving a relation $K_uV \gg k_BT$. However, in a real assembly of magnetic nanoparticles, besides thermal fluctuation, the particle size distribution and also magnetostatic and exchange interactions among the particles become important factors affecting magnetic properties. Recent experimental and theoretical investigations of magnetic particles have been published in review papers.[9–11] The latest computational models[12,13] have treated both the magnetostatic and exchange interactions among magnetic particles, and have shown that coercivity, remanence, and the switching field distribution of magnetic particles depend on the magnetostatic and exchange interactions among the particles.[13]

Tetragonal FePt ordered alloy nanoparticles with an $L1_0$-type ordered structure are now attracting much interest as high-density recording media, because of their large K_u value, as large as 7×10^6 J/m^3 (Ref. 14). High uniaxial anisotropy enables FePt particles to overcome thermal fluctuation even in very small sizes. For $L1_0$-type magnetic alloy nanoparticles, there are additional parameters that affect the

[a]Electronic mail: sato@sanken.osaka-u.ac.jp

magnetic properties, that is, the long-range order parameter. It is known that the order parameter depends both on the annealing condition and alloy composition.[15] According to recent studies on $L1_0$-alloy nanoparticles formed by sputtering or evaporation,[16–20] postannealing at temperatures above 873 K is necessary for the formation of ordered nanoparticles with a large order parameter (that is, large coercivity), since these particles have a metastable disordered alloy structure in their as-prepared form. Such a high-temperature annealing condition is not preferable for industrial application. For the formation of ordered nanoparticles at lower annealing temperatures, several methods, including doping of additive elements, have been performed recently.[21,22] On the contrary, the present authors have reported the formation of oriented $L1_0$-FePd nanoparticles on NaCl(001) at annealing temperatures as low as 773 K,[23] which is 100 K lower than that of FePt particles. The FePd alloy has the K_u value of $2.6 \times 10^6 \mathrm{J/m^3}$,[24] which is a little smaller than that of FePt but larger than that of hcp-Co [$4.53 \times 10^5 \mathrm{J/m^3}$ (Ref. 25)]. In spite of the above advantage compared to FePt, the structure and atomic ordering process of FePd nanoparticles have not been studied so far.

In order to achieve fabrication of the $L1_0$-FePt or FePd nanoparticles suitable for the high-density recording media, suppression of particle coalescence on annealing, control of the size of particles and their *c*-axis orientation, and formation of $L1_0$ nanoparticles at lower temperature are necessary steps to be accomplished. Furthermore, it is necessary to reveal the particle size and order parameter dependences of K_u for $L1_0$ nanoparticles, which have not been made clear yet. For these purposes, it is desirable to clarify the structure and morphology of $L1_0$ nanoparticles in fabricated specimens more in detail, and transmission electron microscopy (TEM) and electron diffraction studies are able to play an important role.

The present study aims at clarifying the structure and morphology changes of FePd nanoparticles on annealing by means of TEM and selected area electron diffraction (SAED). We also study the enhancement of coercivity of FePd nanoparticles on atomic ordering, and using the obtained saturation magnetization, coercivity, and particle size, K_u of the FePd nanoparticles is estimated. Effects of particle size and order parameter on K_u are discussed on recent experimental results for FePt particles[26] and films.[27,28] Change of the remanence on annealing is also discussed compared to a recent theoretical model[14] considering the size distribution and magnetostatic and exchange interactions.

II. EXPERIMENT

Specimen preparation was performed using electron-beam evaporation apparatus (operated at 4 kV) with a base pressure of approximately 3×10^{-7} Pa. Pure Pd (99.95%), Fe (99.97%), and Al_2O_3 (99.99%) crystals were used as evaporation sources. NaCl(001) crystals cleaved in air were supplied as substrates. A quartz thickness monitor attached to the chamber was used to estimate the average thickness of the deposited layer. The process took advantage of the overgrowth of Fe on Pd ''seed'' nanoparticles epitaxially grown on the cleaved NaCl(001) substrates under the substrate temperature of 673 K.[18] After deposition, an amorphous $(a\text{-})Al_2O_3$ film was further deposited at substrate temperatures of about 623 K to protect the particles from oxidation and also to stabilize the particles into the separated condition. The average thickness (and the mean-deposition rate) for Pd, Fe, and Al_2O_3 were 1.5 (0.5), 1 (0.5), and 10 nm (2 nm/min), respectively. According to energy dispersive x-ray spectroscopy (EDS) attached to TEM, the mean composition of the present specimen was found to be Fe–58 at. % Pd. Heat treatments of the as-deposited nanoparticles (hereafter, expressed as Fe/Pd) on the NaCl(001) substrate for the formation of ordered FePd nanoparticles were made in a high-vacuum furnace ($< 2 \times 10^{-5}$ Pa) at 673, 773, 823, and 873 K for 3.6 ks in an Al_2O_3 boat. The heating rate was about 5 K/min. After annealing, the specimen was gradually cooled down to the room temperature in the vacuum furnace with a mean-cooling rate of about 10 K/min. The as-deposited and annealed films (annealed at 773 and 873 K for 3.6 ks) were removed from the NaCl substrate by immersing the substrate into distilled water, and were mounted onto copper grids for TEM observations operated at 200 (JEOL, JEM-2010) and 300 kV (JEOL, JEM-300F). TEM observations of specimen films after annealing on Cu grids without the NaCl(001) substrate were also performed. These TEM specimens were prepared by annealing the as-deposited films at 773 K for 3.6 ks, and 873 K for 3.6 and 36 ks on a Cu grid after removing it from the substrate. For the *in situ* TEM observation of atomic ordering, a specimen heating stage was used. Magnetic hysteresis loops of the FePd nanoparticles on the NaCl(001) substrates after the heat treatments were measured using a superconducting quantum interference device (SQUID) magnetometer (Quantum Design, MPMS-5S).

III. RESULTS

A. Atomic ordering and nanostructure of oriented FePd nanoparticles

TEM images and the corresponding SAED patterns for the as-deposited and annealed (773 and 873 K for 3.6 ks) specimens are shown in Fig. 1. Diffraction spots both from fcc-Pd and bcc-Fe with a mutual fixed orientation can be seen in the SAED pattern in Fig. 1(a). The orientation relationships between the NaCl substrate and Pd, and between Pd and Fe are $[011]_{\mathrm{NaCl}} \| [011]_{\mathrm{Pd}}$, $(100)_{\mathrm{NaCl}} \| (100)_{\mathrm{Pd}}$, and $[100]_{\mathrm{Fe}} \| [100]_{\mathrm{Pd}}, (011)_{\mathrm{Fe}} \| (010)_{\mathrm{Pd}}$, respectively.[18,23] A weak diffuse pattern from the amorphous Al_2O_3 cover layer is also seen in the pattern. In the image in Fig. 1(a) two regions with dark and gray contrasts are observed. The directional dark and gray contrasts were found to be fcc-Pd and bcc-Fe nanoparticle regions, respectively, from the high-resolution TEM (HRTEM) observation, which will be shown later. Superlattice reflections in SAED pattern marked by arrows in the specimen after annealing at 773 K for 3.6 ks [Fig. 1(b)] indicate the formation of an FePd ordered phase. Most of the annealed particles are facetted with edges along ⟨110⟩ FePd. The $L1_0$-FePd nanoparticles fabricated by our method have a size distribution as shown in Fig. 2. The particle size is defined here as the arithmetical mean of the minor and the

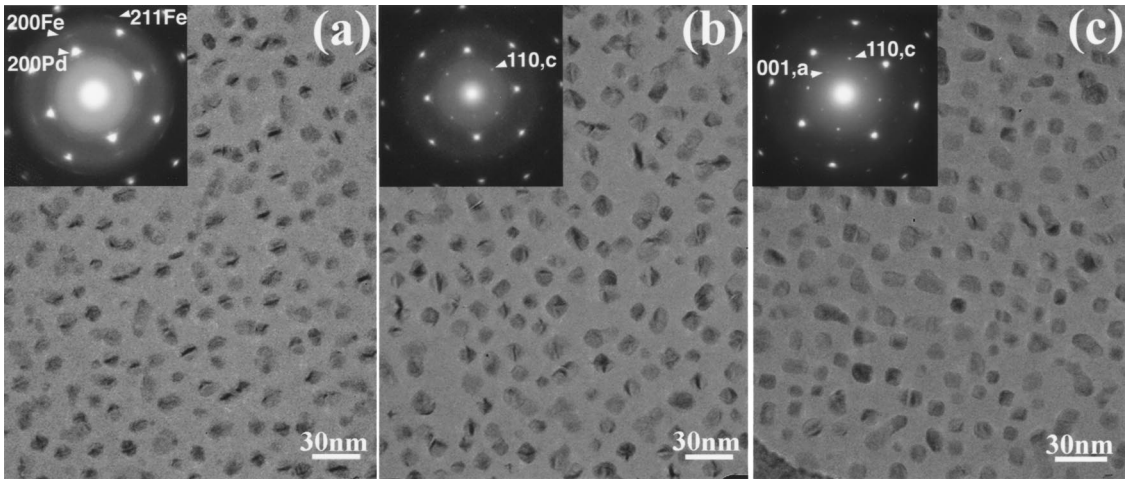

FIG. 1. TEM images and corresponding SAED patterns for as-deposited (a) and annealed specimens [773 K for 3.6 ks (b) and 873 K for 3.6 ks (c)]. Alloying and the atomic ordering reactions were found to occur within each Fe/Pd nanocomplex particle because the particle sizes and the interparticle distances did not change on annealing.

major axes of the ellipse, and the total counting number was 200 from the TEM micrographs. In Fig. 2, the solid curve is a log–normal distribution function. The mean-particle size was 11 nm with the standard deviation of $1n\ \sigma = 0.18$. In the assembly of nanoparticles, it is well known that the size distribution follows a log–normal distribution.[29]

The alloying and the atomic ordering reaction were found to occur within each Fe/Pd nanocomplex particle because the particle sizes and the interparticle distances did not change on annealing. The negligible coalescence can be attributed to an ''anchoring effect'' of the seed Pd to the coalescence growth. It is presumed that the alloying and the atomic ordering reactions proceed simultaneously on annealing since the reflections of both 110_{FePd} (superlattice reflection) and the weak 200_{Fe} reflection coexisted in the SAED pattern after annealing at 773 K for 3.6 ks, and the reflection 200_{Fe} almost disappeared after annealing at 823 K for 3.6 ks. No reflections from the ordered $FePd_3$ phase ($L1_2$ type) was observed on annealing, which shows the ordering process to a thermodynamically stable $L1_0$ structure must be the direct process. Intensity profiles measured along the [001]* direction in the SAED pattern are shown in Fig. 3, indicating the coexistence of Fe and FePd after annealing at 773 K. Lattice parameters were measured from the SAED patterns using a fcc-Pt thin film mounted on a Cu grid as ''standard'' for the camera-length correction in SAED. The measured lattice parameters were $a = 0.381(2)$ and $c = 0.366(1)$ nm and the axial ratio c/a was 0.959(4) for the specimen after annealing at 873 K for 3.6 ks.

We observed the nanostructure change of the FePd nanoparticles during atomic ordering. A HRTEM image of an as-deposited Fe/Pd nanoparticle is shown in Fig. 4. In the particle, crossed lattice fringes from {200} planes of Pd and {011} planes of Fe are visible. The dark contrasts in the central region of the particle run along the $\langle 200 \rangle_{Pd}$ direction. The dark contrasts crossing the particles shown in Fig. 1(a) are, therefore, explained as those from the Pd particles. Annealing of the specimen film on NaCl substrate at 773 K for 3.6 ks in the furnace followed by gradual cooling lead to formation of the $L1_0$-type ordered phase. The {110} lattice fringes with a spacing of 0.27 nm of a tetragonal ordered structure can be seen in the HRTEM image shown in Fig. 5.

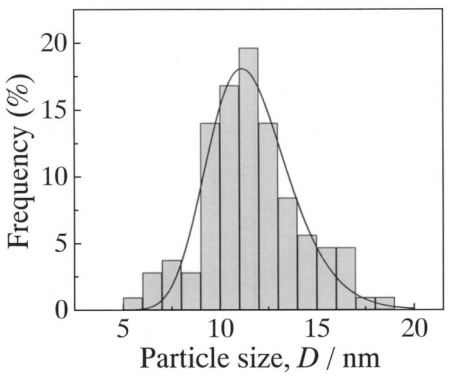

FIG. 2. Particle size distribution for $L1_0$-FePd nanoparticles after annealing at 773 K for 3.6 ks. Solid line indicates the fitting curve by the log–normal distribution function.

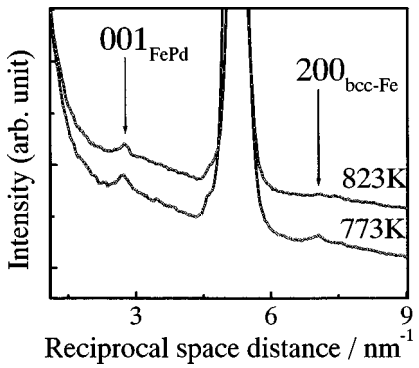

FIG. 3. Diffracted beam intensity profiles for FePd nanoparticles measured along the [001]* direction in the SAED pattern. Reflections of both 110_{FePd} (superlattice reflection) and weak 200_{Fe} (fundamental reflection) coexisted after annealing at 773 K for 3.6 ks, while 200_{Fe} almost disappeared after annealing at 823 K for 3.6 ks. It is presumed that the alloying and the atomic ordering reactions proceed simultaneously on annealing.

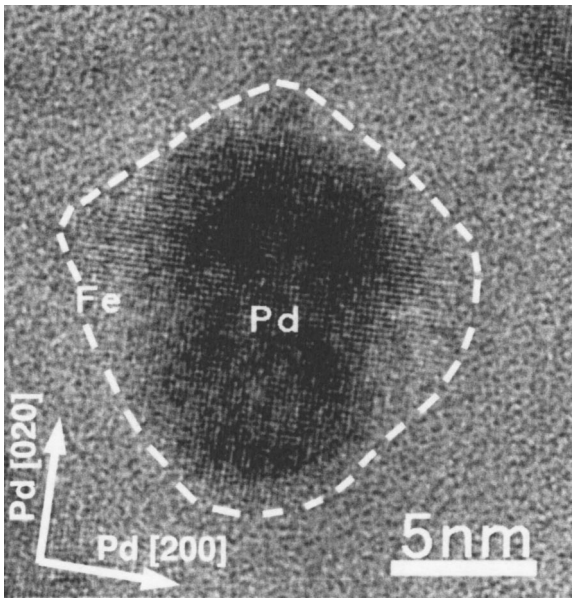

FIG. 4. HRTEM image of an as-deposited Fe/Pd nanoparticle. Crossed lattice fringes from the {200} planes of Pd and {011} planes of Fe are visible.

Different from the case of $L1_0$-FePt nanoparticles,[18] where three-variant domains of the tetragonal $L1_0$ structure coexist with their *c* axes mutually oriented perpendicularly in each nanoparticle, single crystal (single-variant) $L1_0$ nanoparticles were formed by annealing at 773K and particles with their crystallographic *c* axes oriented normal to the film plane are larger in number. This structural feature causes a large perpendicular coercivity of the specimen film as will be discussed later. On annealing the specimen at temperatures above 873 K, particles with their *c* axes parallel to the film plane increased in number in comparison with particles with *c* axes normal to the film plane. The intensity of the superlattice reflections of both 110 and 001 became strong due to

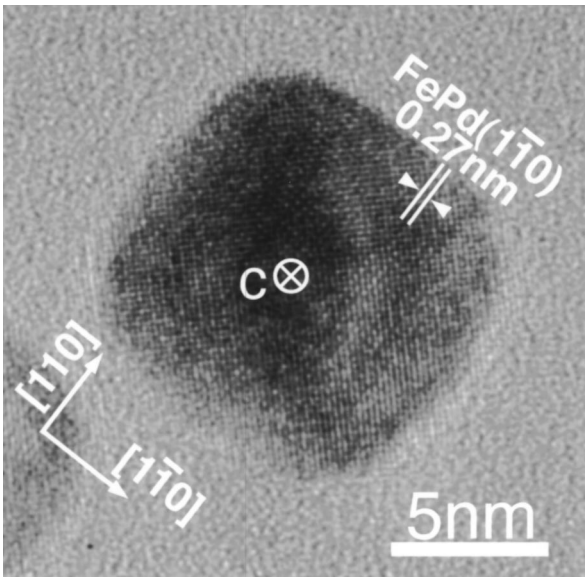

FIG. 5. HRTEM image of an $L1_0$-FePd nanoparticle after annealing at 773 K for 3.6 ks. {110} lattice fringes with spacing of 0.27 nm of tetragonal ordered structure can be seen in the image.

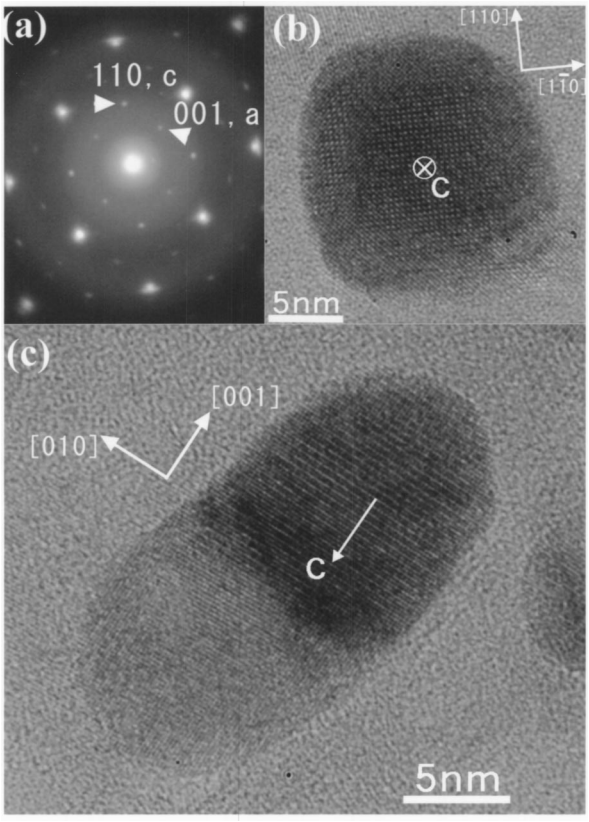

FIG. 6. HRTEM images and the corresonding SAED pattern for FePd nanoparticles after annealing at 873 K for 36 ks. Single-variant structure is found to be a stable form of the tetragonal ordered structure in the present FePd nanoparticles. {110} lattice fringes can be observed in (b) more clearly than those in Figs. 5 due to promotion of the ordering at 873 K.

the proceeding of the atomic ordering. The single-variant structure is considered to be a stable form of the tetragonal ordered structure of the present FePd nanoparticles. It should be noted that the {110} lattice fringes can be observed in Fig. 6(b) more clearly then those in Fig. 5 due to the promotion of the ordering at 873 K. Cheong and Laughlin[30] reported changes of variant volume fraction on annealing until a near-single-variant state was reached in an Fe–45 at. % Pd alloy.

The probability for particle *c*-axis orientation of any one of the three kinds orthogonal variants (two of them oriented parallel to the film plane) is equal if there were no external field. This is because any one of the three ⟨100⟩ axes of the fcc ''seed'' particles can correspond to the tetragonal *c* axis of the $L1_0$ structure. Comparisons of the specimens annealed with and without the NaCl substrate were performed for specimens with annealing temperatures of 773 and 873 K for 3.6 ks in order to examine the substrate effect on the structural change. Figures 7 and 8 show TEM images and the corresponding SAED patterns for specimen annealed at 873 K for 3.6 ks with and without the NaCl substrate. It was found that there are no significant structural differences among them. Further study is needed in order to clarify the tendency of perpendicular orientation of *c* axis in the present FePd nanoparticles.

Some of the particles were composed of two kinds of variants with two different *c* axes and exhibited the structural domains above 873 K while their population was very small

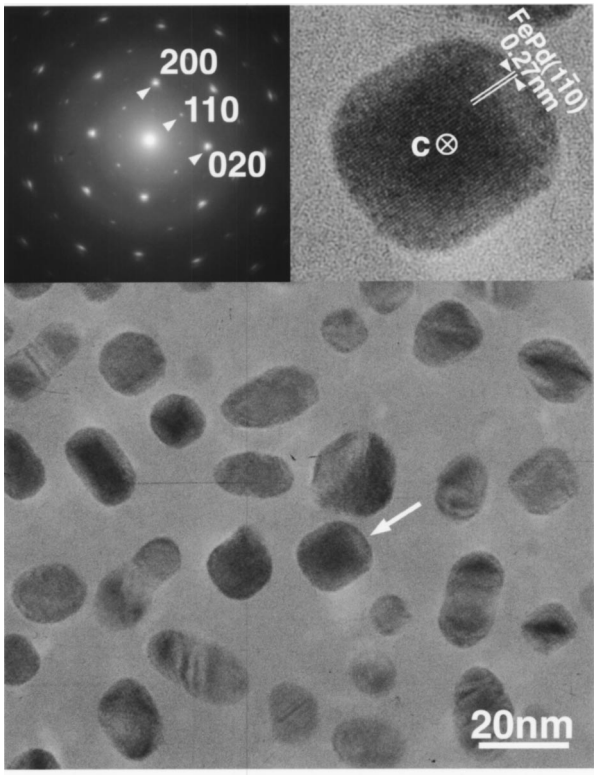

FIG. 7. TEM images corresponding SAED pattern for FePd nanoparticles after annealing at 873 K for 3.6 ks with the NaCl substrate.

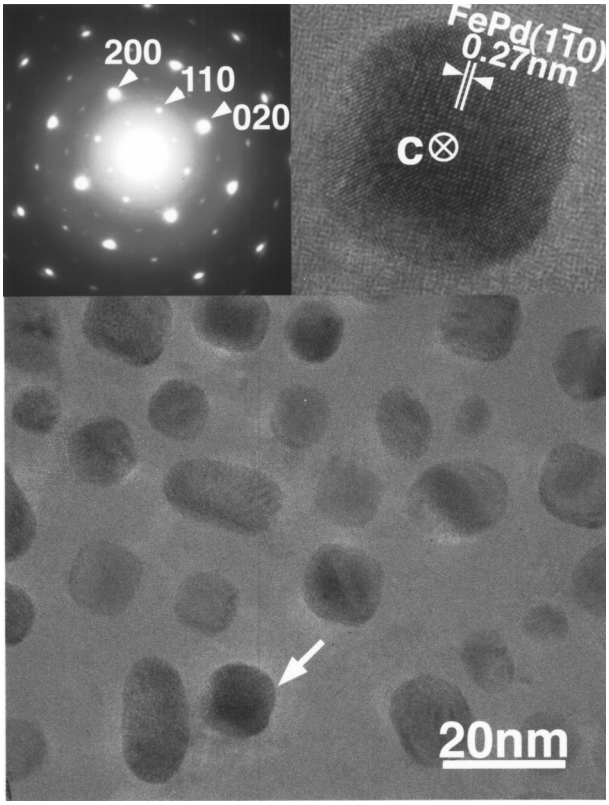

FIG. 8. TEM images and corresponding SAED pattern for FePd nanoparticles after annealing at 873 K for 3.6 ks without the NaCl substrate. There are no significant differences among the FePd specimens annealed with and without the NaCl substrate.

in number and their structure was not largely changed on prolonged annealing at 873 K. Such particles with two variant domains are shown in Figs. 9 (873 K for 3.6 ks) and 10 (873 K for 36 ks). In Figs. 9 and 10 Fourier transforms from the HRTEM images are attached to show the variant structures. From the boundary regions of the two-variant domains in Figs. 9 and 10, it is noted that there are no sharp structural boundaries between the variant domains.

B. Hard magnetic properties due to atomic ordering of oriented FePd nanoparticles

Magnetization curves for as-deposited and annealed (873 K for 3.6 ks) specimens on NaCl(001) substrates are shown in Figs. 11(a) and 11(b), respectively. These magnetization curves were measured at 300 K with the external magnetic field both perpendicular and parallel to the film plane along the cleaved edges of NaCl substrates. Shearing corrections were not performed since an accurate three-dimensional particle shape including the aspect ratio has not been revealed in the present nanoparticles. In Fig. 11(a), small coercivities were obtained both in perpendicular and in-plane directions, and the perpendicular direction was found to be the magnetic hard axis. Since the NaCl substrate was kept at 673 K during the deposition and no significant structural variation was observed by TEM observation at 673 K, bcc-Fe nanoparticles are thought to contribute to the magnetization curve shown in Fig. 11(a). Annealing of the specimen at temperatures above 773 K results in larger coercivities above 1 kOe, which corresponds to the formation of the tetragonal ordered phase with large K_u. In the initial stage of atomic ordering most of the *c* axes of the FePd particles were oriented normal to the film plane, as mentioned in Sec. III A. This structural feature coincides with the characteristics of the magnetization curve for the specimen annealed at 773 K for 3.6 ks, which showed perpendicular and in-plane coercivities of 1.2 and 0.3 kOe, respectively. Annealing at 873 K for 3.6 ks results in the enhancement of perpendicular coercivity (3.5 kOe) due to the development of atomic order as well as the enhancement of in-plane coercivity (2.5 kOe), as shown in Fig. 11(b). The enhancement of in-plane coercivity is attributed to the increase of $L1_0$-FePd nanoparticles with their *c* axes oriented parallel to the film plane in number.

Figure 12 represents the coercivity change on annealing at elevated temperatures between 673 and 873 K for 3.6 ks using a parameter T/T_m, where T_m represents the melting temperature of the Fe–Pd alloy, 1063 K.[31] Open and solid circles represent the coercivities obtained by the magnetization curves measured using magnetic fields applied perpendicular and parallel to the film plane, respectively. Perpendicular coercivities increased above about 0.35 T_m while in-plane coercivities increased above about 0.4 T_m. Figure 12 clearly indicates the fact that ordered phase with the *c* axes oriented normal and parallel to the film plane started to form at temperatures above 0.35 and 0.4 T_m, respectively. The parameter T/T_m would be related to the vacancy concentration for atomic diffusion, and diffusivity is one of the dominant factors for atomic ordering by means of bulk diffusion.

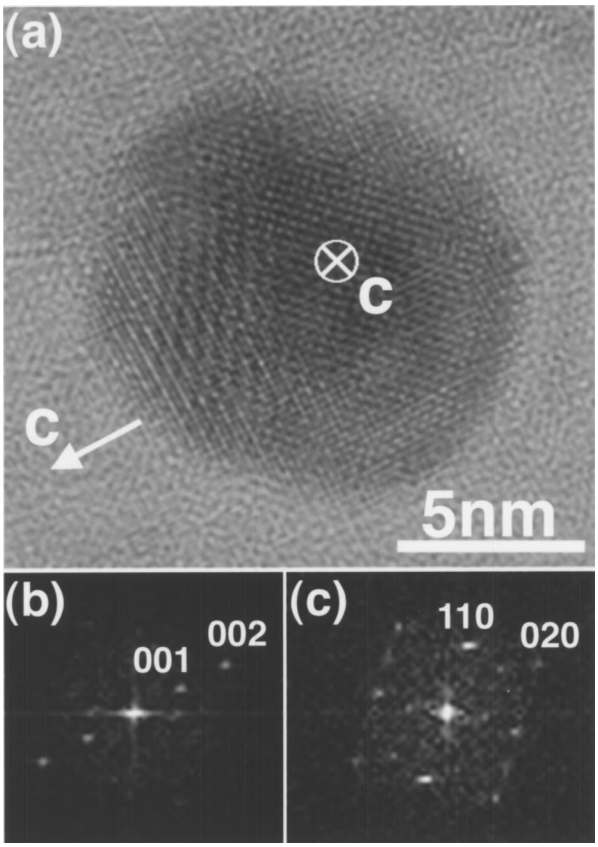

FIG. 9. HRTEM image and Fourier transforms of an FePd nanoparticle with two kinds of variants. Annealing was performed at 873 K for 3.6 ks and observed at 300 K. Some of the particles were composed of such a structural domain. Attached Fourier transforms indicate the existence of two variants in a particle.

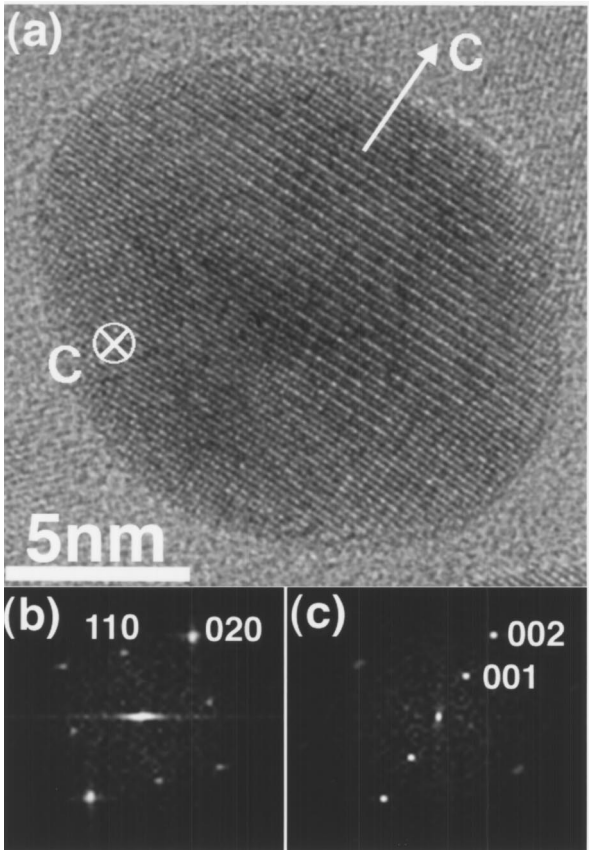

FIG. 10. HRTEM image and Fourier transforms of an FePd nanoparticle with structural domain after annealing at 873 K for 36 ks. FePd particles with structural domains were small in number and their population and structure were not largely changed on prolonged annealing at 873 K.

IV. DISCUSSION

For a random distribution of noninteracting single domain particles with uniaxial anisotropy, coercivity can be calculated using the following Eqs. (2)–(4) by Pfeiffer,[32] assuming coherent rotation of magnetization:

$$H_c = H_{c0}\left[1-\left(\frac{V_S}{V}\right)^{0.77}\right] \tag{2}$$

$$V_S = \frac{25k_BT}{K_u} \tag{3}$$

$$H_{c0} = 0.96\frac{K_u}{I_s}, \tag{4}$$

where the volume for the superparamagnetic limit is denoted by V_s. Here, we defined V as $\pi D^3/6$ (D: particle size). The relaxation frequency is assumed to be 10^9 s^{-1} and the thermal relaxation time of spins is set to be 10^2 s. Using this equation, estimation of the coercivity was reported for randomly oriented Co (Ref. 33) and CoPt particles.[33–35] We performed the calculation of coercivity for 10-nm-sized FePd nanoparticles with a random distribution. In the calculation, K_u of 2.6×10^6 J/m^3 and I_s of 1100 emu/cm^3 were assumed.[24] A coercivity value of 10 kOe at 300 K is obtained. In spite of the development of the atomic ordering, the obtained coercivity is still smaller than the expected value. K_u for the present FePd nanoparticles is thought to be smaller than that of the bulk FePd alloy. In this study the K_u of the present FePd nanoparticles was estimated for perpendicular and in-plane magnetization curves using the Eqs. (2)–(4), since the magnetization curves shown in Figs. 11(a) and 11(b) resemble the magnetization curves for randomly distributed particles in spite of the existence of three orthogonal directions in c axes orientation. In these calculations, specimen film thickness was estimated to be 3.1 nm for Fe and Pd as a continuous film in order to estimate the saturation magnetization of the FePd nanoparticles. The numerical values obtained are listed in Table I. The difference in K_u values between the perpendicular and in-plane cases can be attributed to the epitaxial growth of FePd nanoparticles, that is, the particles are not randomly distributed but have three orthogonal orientations along the principal axis of the NaCl(001) substrate. The obtained K_u is smaller than that of the bulk $L1_0$-FePd [2.6×10^6 J/m^3 (Ref. 24)]. Besides the small value of K_u, there must be another reason for the present smaller coercivity. A slight shoulder of the magnetization curves near the remanence [see Fig. 11(b)] indicates an existence of the $L1_0$-FePd particle with different K_u.[34,35] The variety of K_u is thought to be due to the distribution of the alloy composition with the particles, which results in different degrees of atomic order from particle to particle.

As for the relation between the order parameter (S) and K_u in $L1_0$-type ordered alloys, Markov *et al.*[36] reported the

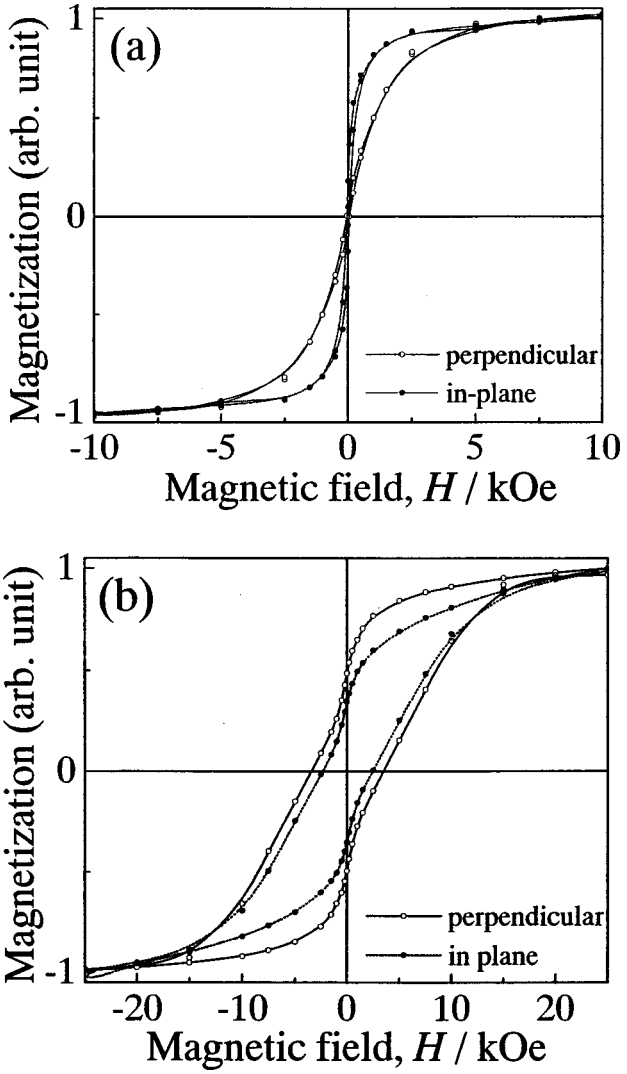

FIG. 11. Magnetization curves for as-deposited (a) and annealed (b) specimens on NaCl(001) substrates. Magnetization curves were measured at 300 K with the external field both perpendicular (open circles) and parallel (solid circles) to the film plane along the principal axes of the NaCl substrates. Shear correction was not made for the perpendicular magnetization curve.

correlation $K_u \propto S^2$ for their single crystal CoPt and FePd alloys. Recently, for FePt films, Kanazawa *et al.*[27] and Okamoto *et al.*[28] have reported the gradual increase of K_u with increasing S. Shima *et al.*[26] have reported a decrease of K_u with decreasing film thickness below 25 nm thick, which corresponds to the particle size reduction. They also indicated that the morphology changed from maze-like discontinuous particles isolated particles to in the region with a film thickness of 45 nm. It is obvious that both the order parameter and particle size affect K_u, while there is no report on the order parameter and size effects on K_u for 10-nm-sized $L1_0$ alloy particles. A correct estimation of the order parameter for the present FePd nanoparticles is now in progress.

Normalized remanences of the present FePd particles were 0.5(perpendicular) and 0.35 (in plane), as shown in Table 1. The SW model[5] predicted the remanence of 0.5 for noninteracting particles. A recent computational model has shown that remanence is greatly changed by both magnetostatic and exchange interactions among particles.[14] For example, considering only the magnetostatic interaction, (1) the remanence is smaller than 0.5 depending on the packing density (p), while (2) the remanence is enhanced for higher K_u.[14] In the present study, the contribution of the interparticle exchange interaction is negligible, since each FePd nanoparticle is well isolated (see Fig. 1). We determined p of our specimen as about 0.3 using TEM micrographs. For FePd nanoparticles after annealing at 773 K for 3.6 ks (with smaller coercivity, see Fig. 12), the remanences were 0.35 (perpendicular) and 0.2 (in plane). Smaller coercivity corresponds to the smaller K_u, since p did not change during annealing (see Fig. 1). So, it can be said that particles with larger K_u have larger remanence, which agrees qualitatively with the above features (1) and (2) predicted by the numerical model.[14] The increase of remanence on annealing is explained by the enhancement of K_u due to the proceeding of atomic ordering. Kechrakos and Trohidou[37] also presented the K_u dependence of the remanence by considering the magnetostatic interaction.

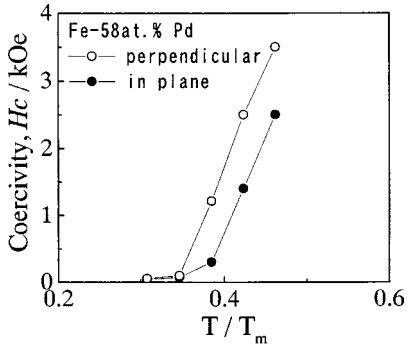

FIG. 12. Coercivity change on annealing at elevated temperatures between 673 and 873 K for 3.6 ks using a parameter T/T_m, where T_m represents the melting temperature of the Fe–Pd alloy. Perpendicular and in-plane coercivities increased at annealing temperatures above $0.35T_m$ and $0.4T_m$, respectively.

V. CONCLUSION

10-nm-sized isolated $L1_0$-FePd nanoparticles with orientation have been fabricated and large coercivities as large as 3.5 kOe were obtained at 300 K. In our fabrication method, grain growth of the FePd particles during annealing was greatly suppressed and the isolation of the particles was kept after the ordered phase formation. The negligible coalescence can be attributed to an ''anchoring effect'' of the seed Pd to the coalescence growth. Alloying and atomic ordering reactions proceeded almost simultaneously by postannealing

TABLE I. Particle size (D), coercivity (H_c), saturation magnetization (I_s), magnetoanisotropy constant (K_u), and residual magnetization ratio (I_r/I_s) for FePd nanoparticles after annealing at 873 K for 3.6 ks. The mean composition was Fe–58 at. % Pd. Shear correction was not made for the perpendicular magnetization curve.

	D/nm	H_c/ kOe	I_s/ emu cm^{-3}	Ku/ J m^{-3}	I_r/I_s
Perpendicular	11	3.5	1050	1.0×10^6	0.50
In plane	11	2.5	980	7.7×10^5	0.35

at temperatures between 723 and 823 K. Most of the annealed particles are single crystal with *c* axes oriented both normal and parallel to the film plane, which is different from the case of FePt nanoparticles with three-variant domain structures extending in each particle. It was found that the NaCl substrate did not affect the atomic ordering process in FePd nanoparticles. According to Pfeiffer's equation, coercivity of 10 kOe at 300 K is expected for 10-nm-sized FePd nanoparticles assuming K_u and I_s for bulk alloys. The relatively lower coercivity of the present FePd nanoparticles than that expected from the theoretical model can be explained by the lower value of K_u compared with bulk FePd. Both the order parameter and particle size are thought to affect K_u, considering recent experimental results on FePt films and particles. Precise determination of the order parameter in 10-nm-sized particles is now in progress. The change of remanence on annealing agreed qualitatively with the result by the recent computational model considering the size distribution and magnetostatic and exchange interactions among the particles. The present specimen fabrication method is useful for fabricating $L1_0$ nanoparticles with a smaller size distribution and particle isolation without coalescence. Though the epitaxial growth of FePd nanoparticles on the cleaved NaCl substrate has the advantage of *c*-axes orientation compared to polycrystalline nanoparticles, it is still necessary to control the *c*-axis orientation of the particles in one direction for future ultra-high-density magnetic recording media. Formation of $L1_0$ ordered particles with large coercivity under lower temperature is also desired, though the present FePd nanoparticles showed a coercivity larger than 1 kOe after annealing at 773 K, which is 100 K lower than that of FePt or CoPt nanoparticles.

ACKNOWLEDGMENTS

The authors wish to thank Professor T. Kawai and Dr. H. Tanaka of ISIR, Osaka University, for supporting the SQUID measurement. This study was supported by the Center of Excellence (COE) program at ISIR, Osaka University, and the Grant-in-Aid for Scientific Research (Nos. 14205094, 13555189 and 13750612) from the Japanese Ministry of Education, Culture, Sports, Science and Technology.

[1] E. S. Murdock, IEEE Trans. Magn. **28**, 3078 (1992).
[2] D. N. Lambeth, E. M. T. Velu, G. H. Bellesis, L. L. Lee, and D. E. Laughlin, J. Appl. Phys. **79**, 4496 (1996).
[3] M. H. Kryder, MRS Bull. **21**, 17 (1996).
[4] R. L. White, R. M. H. New, and R. F. W. Pease, IEEE Trans. Magn. **33**, 990 (1997).
[5] E. S. Stoner and E. P. Wohlfarth, Philos. Trans. R. Soc. London, Ser. A **240**, 599 (1948).
[6] L. Néel, Ann. Geophys. (C.N.R.S.) **5**, 99 (1949).
[7] *Selected Works of Louis Néel*, edited by N. Kurti (Gordon and Breach, London, U.K., 1988).
[8] C. P. Bean and J. D. Livingston, J. Appl. Phys. **30**, 120S (1959).
[9] *Magnetic Properties of Fine Particles*, edited by J. L. Dormanh and D. Fiorani (North-Holland, Amsterdam, 1992).
[10] *Applied Magnetism*, edited by R. Gerber, C. D. Wright, and G. Asti (Kluwer, Dordrecht, The Netherlands, 1994), p. 113.
[11] J. L. Dorman, D. Fiorani, and E. Tronc, Adv. Chem. Phys. **98**, 283 (1997).
[12] M. El-Hilo, R. W. Chantrell, and K. O'Grady, J. Appl. Phys. **84**, 5114 (1998).
[13] C. Verdes, B. Ruiz-Diaz, S. M. Thompson, R. W. Chantrell, and Al. Stancu, Phys. Rev. B **65**, 174417 (2002).
[14] O. A. Ivanov, L. V. Solina, V. A. Demshila and L. M. Magat, Phys. Met. Metallogr. **35**, 92 (1973).
[15] B. E. Warren, *X-ray Diffraction* (Dover, New York, 1969), p. 208.
[16] C. Chen, O. Kitakami, and Y. Shimada, IEEE Trans. Magn. **35**, 3466 (1999).
[17] T. Shimatsu, J. C. Lodder, Y. Sugita, and Y. Nakamura, IEEE Trans. Magn. **35**, 2697 (1999).
[18] B. Bian, K. Sato, Y. Hirotsu, and A. Makino, Appl. Phys. Lett. **75**, 3686 (1999).
[19] C. P. Luo and D. J. Sellmyer, Appl. Phys. Lett. **75**, 3162 (1999).
[20] M. Watanabe, T. Masumoto, D. H. Ping, and K. Hono, Appl. Phys. Lett. **76**, 3971 (2000).
[21] C. Chen, O. Kitakami, S. Okamoto, and Y. Shimada, Appl. Phys. Lett. **76**, 3218 (2000).
[22] D.H. Ping, M. Ohnuma, K. Hono, M. Watanabe, T. Iwasa, and T. Masumoto, J. Appl. Phys. **90**, 4708 (2001).
[23] K. Sato, B. Bian, and Y. Hirotsu, Jpn. J. Appl. Phys., Part 2 **39**, L1121 (2000).
[24] A. Kussmann and K. Müller, Z. Angew. Phys. **17**, 509 (1964).
[25] R. Pauthenet, Y. Barnier, and G. Rimet, J. Phys. Soc. Jpn. **17**, 309 (1962).
[26] T. Shima, K. Takanashi, Y. K. Takahashi, and K. Hono, Appl. Phys. Lett. **81**, 1050 (2002).
[27] H. Kanazawa, G. Lauhoff, and T. Suzuki, J. Appl. Phys. **87**, 6143 (2000).
[28] S. Okamoto, N. Kikuchi, O. Kitakami, T. Miyazaki, and Y. Shimada, Phys. Rev. B **66**, 024413 (2002).
[29] C. G. Granqvisst and R. A. Buhrman, J. Appl. Phys. **47**, 2200 (1976).
[30] B. Cheong and D. E. Laughlin, Scr. Metall. Mater. **29**, 829 (1993).
[31] *Binary Alloy Phase Diagrams*, 2nd ed., edited by T. B. Massalski, H. Okamoto, P. R. Subramanian, and L. Kacprzak (ASM International, Materials Park, OH, 1990), p. 1751.
[32] H. Pfeiffer, Phys. Status Solidi A **118**, 295 (1990).
[33] T. Ibusuki, O. Kitakami, Y. Endo, S. Okamoto, and Y. Shimada, Scr. Mater. **44**, 1327 (2001).
[34] S. Stavroyiannis, I. Panagiotopoulos, D. Niarchos, J. A. Christodoulides, Y. Zhang, and G. C. Hadjipanayis, Appl. Phys. Lett. **73**, 3453 (1998).
[35] I. Panagiotopoulos, S. Stavroyiannis, D. Niarchos, J. A. Christodoulides, and G. C. Hadjipanayis, J. Appl. Phys. **87**, 4358 (2000).
[36] V. V. Maykov, A. Ye. Yermakov, G. V. Ivanov, V. I. Khrabrov, and L. M. Magat, Phys. Met. Metallogr. **67**, 76 (1989).
[37] D. Kechrakos and K. N. Trohidou, Phys. Rev. B **58**, 12169 (1998).